Nucleic Acids Research, 2024, 1–13
https://doi.org/10.1093/nar/gkae108
Nucleic Acid Enzymes

Communication between DNA and nucleotide binding sites facilitates stepping by the RecBCD helicase

Vera Gaydar, Rani Zananiri, Layla Saied, Or Dvir, Ariel Kaplan and Arnon Henn*

Faculty of Biology, Technion - Israel Institute of Technology, Haifa 3200003, Israel

*To whom correspondence should be addressed. Tel: +972 48294839; Fax: +972 778871913; Email: arnon.henn@technion.ac.il

Abstract

Double-strand DNA breaks are the severest type of genomic damage, requiring rapid response to ensure survival. RecBCD helicase in prokaryotes initiates processive and rapid DNA unzipping, essential for break repair. The energetics of RecBCD during translocation along the DNA track are quantitatively not defined. Specifically, it's essential to understand the mechanism by which RecBCD switches between its binding states to enable its translocation. Here, we determine, by systematic affinity measurements, the degree of coupling between DNA and nucleotide binding to RecBCD. In the presence of ADP, RecBCD binds weakly to DNA that harbors a double overhang mimicking an unwinding intermediate. Consistently, RecBCD binds weakly to ADP in the presence of the same DNA. We did not observe coupling between DNA and nucleotide binding for DNA molecules having only a single overhang, suggesting that RecBCD subunits must both bind DNA to 'sense' the nucleotide state. On the contrary, AMPpNp shows weak coupling as RecBCD remains strongly bound to DNA in its presence. Detailed thermodynamic analysis of the RecBCD reaction mechanism suggests an 'energetic compensation' between RecB and RecD, which may be essential for rapid unwinding. Our findings provide the basis for a plausible stepping mechanism' during the processive translocation of RecBCD.

Graphical abstract

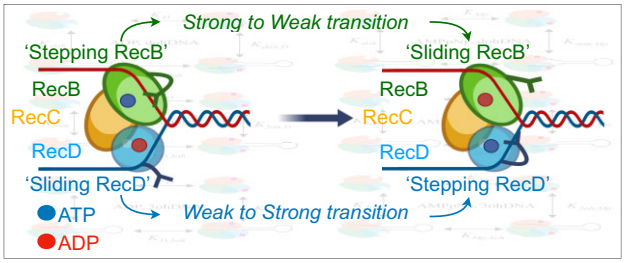

Introduction

Double-strand DNA breaks (DSDBs) are the severest type of genome damage, requiring fast and efficient repair (1). Helicases play an essential role in the repair mechanisms of DSDBs in every living organism (2). In prokaryotes, members of the RecBCD family unwind DSBs in preparation for strand invasion, which is essential for repair by homologous recombination (3). RecBCD is a highly processive DNA helicase exhibiting an exceptionally high unwinding rate of ∼ 1600 base pairs (bp) per second (s^{-1}) (4). RecBCD is a heterotrimer composed of one copy of RecB, RecC and RecD, out of which RecB and RecD are DNA translocases and helicases (5–7). The RecC subunit 'staples' the RecB and RecD subunits (8) and is crucial in destabilizing the duplex DNA ahead of the translocase activities of RecB and RecD (9) and recognizing the regulatory Chi sequence (10). RecBCD catalyzes ssDNA translocation on opposite DNA polarities, with RecB moving on the 3′ → 5′ strand and RecD moving on the 5′ → 3′ strand, resulting in net translocation of RecBCD complex along the duplex DNA (6,11,12). RecBCD can also push through a highly crowded protein environment while maintaining processivity, providing an additional enzymatic adaptation to its mechanism (13,14). Although repair mechanisms for DSBs are present in all living organisms, there is no known eukaryotic homolog of RecBCD in terms of its structural organization and rapid, processive unwinding.

For RecBCD to transverse processively with the two motors translocating along the individual strands of the DNA, a stepping-like mechanism is most likely required. For example, a simple alternation between strong and weak DNA binding states can support processive translocation (15–17). The continuous threading and sliding of ssDNA through the proposed DNA tunnels or cavities in RecBCD will most likely advance via alteration between attached (strong binding state) and detached (weak binding) states. In this sense, RecBCD could function as a double-headed ATPase molecular machine, i.e. a molecular motor that has two motors that transverse along the DNA lattice, in analogy to double-headed

Received: May 22, 2023. **Revised:** January 30, 2024. **Editorial Decision:** January 31, 2024. **Accepted:** February 5, 2024

molecular motors such as myosin V, which has been shown to perform processive stepping along the actin filament by walking 'hand over hand' (18–20). Threading ssDNA through a semi-open DNA tunnel that forms in RecB and partially in RecD will increase processivity but still requires cycles of coordinated association-dissociation transitions to permit net vectorial translocation (21). The bound nucleotide state (ATP, ADP-P_i, or ADP) may support such a mechanism by modulating the motor affinities towards the lattice it traverses on, as shown for all myosins and kinesins, as for some helicases (22–28). However, the extent by which nucleotide binding modulates the affinity of RecBCD towards DNA is yet to be examined.

Biochemical and structural studies of RecBCD provide a framework to study how the interactions between RecBCD and the DNA are modulated for translocation and unwinding to progress at high velocities (29). Using a nuclease protection (footprinting) assay, Smith and coworkers showed that within the unwinding initiation complex the DNA ends are protected: ∼21 nucleotides on the 5′ end by RecCD and ∼17 nucleotides on the 3′ strand by RecB (30). This was the first evidence that both strands engage with both helicase subunits of RecBCD, which provide an essential basis for any unwinding model by RecBCD. Later, using a higher resolution footprinting technique, the overall length of the DNA was shown to be ∼21–22 nucleotides, being partially dsDNA and then ssDNA beyond the pivotal RecBCD strcutural motif splitting the dsDNA (31). This posed additional challenges to dissecting the modulation of different DNA structures accurately with respect to the nucleotide state because of the numerous contact sites of the DNA bases with specific amino acids along the DNA binding sites. Recently, a structural analysis of RecBCD with DNA duplex carrying a chi sequence using high-resolution cryo-EM shows numerous molecular interactions throughout the RecBCD complex (32). This RecBCD-duplex DNA structure is unique due to the presence of the Chi sequence inducing notable conformational changes in RecBCD and a compact interaction. Hence, it can also be assumed that any duplex DNA will also have a pronounced grip along the cavities of RecBCD for the DNA strands. Finally, rapid threading of ssDNA throughout RecB and RecCD cavities without provoking large domain and conformational changes to allow rapid and processive unwinding is yet to be demonstrated, i.e. the biochemical states need to be related to the unwinding steps.

In this work, we systematically determined the affinity of RecBCD for DNA substrates in the presence and absence of nucleotides. We characterized RecBCD's binding to diverse DNA substrates and nucleotides, mimicking intermediate states along its unwinding reaction cycle to reveal the nucleotide-binding linkage within RecBCD. Our results suggest that an ADP-bound biochemical intermediate, where strong coupling between DNA and ADP binding is observed, is essential to allow stepping during the translocation of RecBCD.

Materials and methods

Reagents, expression and purification of RecBCD

All chemicals and reagents were the highest purity commercially available. ATP and ADP were purchased from Roche Molecular Biochemicals (Indianapolis, IN, USA). Adenosine 5′-(β,γ-imido)triphosphate (AMPpNp) was purchased from Sigma (St. Louis, MO, USA). A molar equivalent of $MgCl_2$ was added to nucleotides immediately before use. Nucleotide concentrations were determined by absorbance using an extinction coefficient e_{259} of 15 400 M^{-1} cm^{-1}. The concentrations of N-methylanthraniloyl (mant) derivatives of ADP, 2′-deoxyADP, ATP, and 2′-deoxyATP (Jena Bioscience, Jena, Germany) were determined using e_{255} of 23 300 M^{-1} cm^{-1}. Unless otherwise specified, all experiments were conducted in RecBCD Buffer (RB: 20 mM MOPS pH 7.4, 75 mM NaCl, 2 mM $MgCl_2$, 1 mM DTT). Over-expression and purification of recombinant WT RecBCD and mutant $RecB^{K29Q}C$ were based on the previously described method (33,34), with an additional step described by Zananiri *et al.* (35). The RecBCD concentration was determined using $e_{280} = 4.2 \times 10^5$ M^{-1} cm^{-1} in guanidinium chloride. RecBCD purity of nucleic acid contaminants was determined by measuring the absorption ratio of 280/260 nm, and only protein fractions with a ratio >1.3 were used.

DNA substrates preparations

DNA oligonucleotides were purchased from IDT (Leuven, Belgium) and were HPLC purified. The DNA substrates are shown in Supplementary Figure S1. All DNA used in the binding experiments was obtained by folding or hybridizing the DNA in 20 mM MOPS pH 7.4, 75 mM NaCl and 1 mM $MgCl_2$ buffer at 85°C for 3 min, followed by slow cooling to room temperature before storage at –20°C.

DNA binding measurements by fluorescence anisotropy (FA)

FA measurements were performed with a PC1 spectrofluorometer set up in a T-format configuration for simultaneous acquisition on two emission channels using monochromators equipped with automatic polarizers. Samples were equilibrated in RB for 60 min at RT and then measured with $\lambda_{ex} = 492$ nm using vertically polarized light. The emitted vertical and horizontal polarized light was monitored at 90° with emission monochromators at $\lambda_{em} = 523$ nm at 25 ± 0.1°C. The instrument manufacturer calculated the g-factor to correct the gains between vertical and horizontal PMT detectors. Nucleotide concentrations in the indicated measurements were 2 mM (Mg•ADP, or Mg•AMPpNp) at saturation. Fluorescent DNA substrates were held at a constant concentration of 25 nM.

RecBCD oligomeric state and stoichiometric binding isotherms

To rule out the existence of a dimer of RecBCD during substrate binding, we determined the oligomeric state of RecBCD under our experimental conditions, similar to what had been performed earlier (10). Supplementary Figure S2A shows the stoichiometric binding of ssDNA and hpDNA (Supplementary Figure S1 and Supplementary Table S1) under the condition in which [DNA] >> K_D and RecBCD is titrated well above the K_D (Table 1) measured by FA (Figure 1A) and fitted according to Eq. 1:

$$[RecBCD \cdot DNA] = \frac{(R + n + \frac{K_D}{[DNA]_T} + \sqrt{\left(R + n + \frac{K_D}{[DNA]_T}\right) - 4R \cdot n}}{2n} \quad (1)$$

Table 1. Equilibrium constants for DNA substrates binding to RecBCD and RecBCD·nucleotides complex

Equilibrium Constant	Complex structure	DNA substrate binding	[1]K_D (nM)	Complex annotation	$\Delta G°'_{association}$ (kJ·mol^{-1})	
K_{hp}		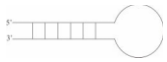	42 ± 9	RecBCD·hpDNA-F	- 42.1 ± 0.5	
$K_{hp, A}$			85 ± 19	RecBCD·AMPpNp·hpDNA-F	- 40.3 ± 0.6	
$K_{hp, D}$			127 ± 31	RecBCD·ADP·hpDNA-F	- 39.3 ± 0.6	
K_{doh}		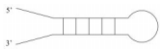	19.2 ± 5	RecBCD·dohDNA-F	- 44.0 ± 0.6	
$K_{doh, A}$			34.0 ± 7.0	RecBCD·AMPpNp·dohDNA	- 42.6 ± 0.5	
$K_{doh, D}$			823.0 ± 261.0	RecBCD·ADP·dohDNA	- 34.7 ± 0.8	
K_{5oh}			29.6 ± 7	RecBCD·5ohDNA-F	- 43.0 ± 0.6	
$K_{5oh, A}$			31 ± 8	RecBCD·AMPpNp·5ohDNA-F	- 43.0 ± 0.6	
$K_{5oh, D}$			8 ± 2	RecBCD·ADP·5ohDNA-F	- 46.2 ± 0.6	
K_{3oh}		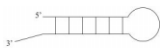	92.6 ± 15.4	RecBCD·3ohDNA-F	- 40.1 ± 0.4	
$K_{3oh, A}$			166.3 ± 41	RecBCD·AMPpNp·3ohDNA-F	- 38.7 ± 0.6	
$K_{3oh, D}$			16.3 ± 7	RecBCD·ADP·3ohDNA-F	- 44.4 ± 1.1	
K_{ss}			7 ± 2	RecBCD·ssDNA-F	- 46.6 ± 0.5	
$K_{ss, A}$			4.5 ± 2	RecBCD·AMPpNp·ssDNA-F	- 47.6 ± 1.8	
$K_{ss, D}$			13 ± 5	RecBCD·ADP·ssDNA-F	- 45.0 ± 0.2	
					Hill plot	n_H
K_{ss}			16.5 ± 3.1	RecBCD·ssDNA-F	- 44.4 ± 0.5	1.4 ± 0.32
$K_{ss, A}$			7.0 ± 5.0	RecBCD·AMPpNp·ssDNA-F	- 46.5 ± 1.8	0.7 ± 0.20
$K_{ss, D}$			23.1 ± 2.2	RecBCD·ADP·ssDNA-F	- 43.6 ± 0.2	2.1 ± 0.34

[1]Equilibrium constants reflect the macroscopic binding affinity of DNA binding to the RecBCD).
RecB, RecC and RecD are shown as oval shapes in orange, green, and light blue, respectively; ATP and ADP are drawn as spheres in blue and red, respectively.

Under stoichiometric conditions of $[DNA]_T >> K_D$, R is the plotted (experimental) mole/mole ratio of RecBCD/DNA, n is the ratio of the fit of RecBCD to DNA, and the DNA_T is the DNA (ssDNA or hpDNA) concentration. The analysis shows that RecBCD:hpDNA and RecBCD: ssDNA bind with 1:1 and 1:2 stoichiometric ratios. Previously, the stoichiometry binding of fluorescently labeled single-stranded overhang (Supplementary Figure S1C) had a similar stoichiometry ratio to the RecBCD heterotrimer (36).

Analysis by analytic size exclusion chromatography (SEC)

RecBCD•hpDNA complex in comparison to RecBCD (SI Figure 2B) clearly shows a monodispersed peak of approximate MW of ∼330 kDa (determined by the linear range of known MW protein marker) in complex with the major peak of the hpDNA with a ratio of 1:1, 280:260 nm absorbance (in comparison to only RecBCD of 3:1, 280:260 ratio). This further confirms the RecBCD: hpDNA stoichiometry to be 1:1.

DNA binding isotherms for K_D determination

Model 1

The binding of DNA substrates to RecBCD is described by the following stoichiometric reaction scheme (Scheme 1):

$$RecBCD + xDNA \overset{K_D}{\leftrightarrow} RecBCD \cdot xDNA \quad \text{(Scheme 1)}$$

where xDNA can be any of the DNA substrates used in this work.

The general solution for this equilibrium binding scheme is in the form of the following quadratic Eq. (2):

$$[RecBCD \cdot xDNA] = ([RecBCD]_T + [xDNA]_T + K_D) + \sqrt{\frac{\left(([RecBCD]_T + [xDNA]_T + K_D)^2 - 4[RecBCD]_T \cdot [xDNA]_T\right)}{2}} \quad (2)$$

where $[DNA]_T$ is the monitored species, $[RecBCD]_T$ is the titrated species, [RecBCD•xDNA] is the bound species. For FA measurements, the premise is that the total fluorescence intensity remains constant throughout the titration (37,38). Under our measurement conditions, the changes in the FTI were minimal to be neglected, allowing the direct fitting of the FA binding isotherm curve using Eq. (2) to determine the equilibrium binding constants.

Model 2

The analysis of ssDNA binding to RecBCD using a Hill equation reveals cooperativity in DNA binding in the presence of ADP to RecBCD, and this is shown in Scheme 2, Eq. (3):

$$RecBCD + ssDNA \overset{K_D}{\leftrightarrow} RecBCD \cdot (ssDNA)_2 \text{(Scheme 2)}$$

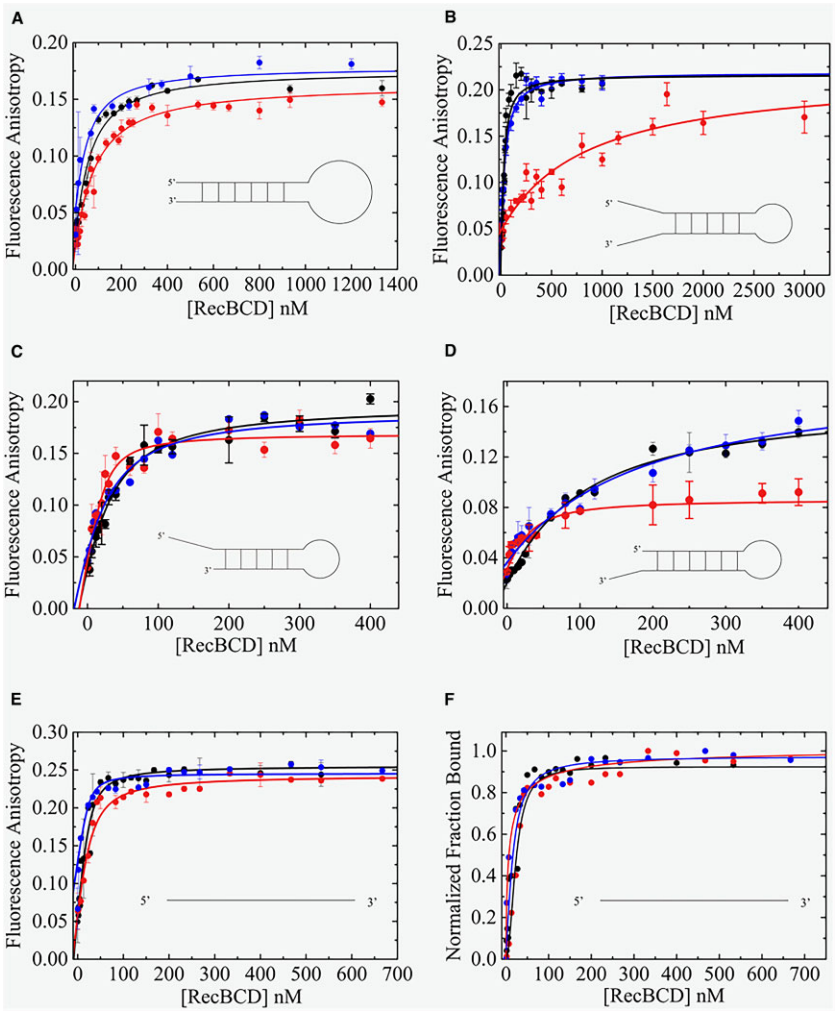

Figure 1. Fluorescence Anisotropy equilibrium binding measurements of RecBCD and RecBCD × nucleotide complexes to fluorescently labeled DNA. DNA substrates were labeled with 6-fluorescein amidite. Fluorescent DNA was held at 25 nM, and RecBCD was titrated to reach saturation of the binding isotherm. Binding to RecBCD (•), RecBCD × AMPPpNp (•), and RecBCD × ADP (•) is shown for (**A**) hpDNA, (**B**) dohDNA, (**C**) 5ohDNA, (**D**) 3ohDNA and (**E**) ssDNA. $\lambda_{ex} = 492$ nm and $\lambda_{em} = 523$ nm. Nucleotide concentrations where indicated were 2 mM (Mg × ADP, or Mg × AMPPpNp). (**F**) Data in (B) fitted to a Hill equation. Error bars report the s.d. of $n = 3$ independent measurements. Lines through the data points are the best fit for Eq. (2).

To extract the two parameters K_H and n_H as shown in Eq. (3):

$$\theta = \frac{[RecBCD]^n}{[RecBCD]^n + [K]^n} \quad (3)$$

where θ is the fraction bound K is the apparent dissociation constant, and n is the Hill coefficient, assuming that the ssDNA binding sites are similar but not identical.

mantNucleotide binding to RecBCD by Förster resonance energy transfer (FRET):

FRET measurements were performed using a PC1 spectrofluorometer (ISS, Champaign, IL) with excitation and emission monochromators. The observation cell was regulated with a Peltier temperature controller at 25 ± 0.1°C. All equilibrium binding reactions were performed in a 10 μl Precision cell fluorescence cuvette (Farmingdale, NY, USA), which allows minimal inner filter effects up to a concentration of ∼550 mM mantNucleotides. Reactions were performed in RB, and mantNucleotides at the specified concentration were prepared with an equal concentration of $MgCl_2$ (1:1 stoichiometric ratio) before being added to RB (35). Equilibrium binding reactions of mantNucleotides to RecBCD were measured by FRET between RecBCD intrinsic tryptophan fluorescence ($\lambda_{ex} = 280$ nm) and bound mantNucleotide (fluorescence monitored at 90° through an emission monochromator at $\lambda_{em} = 436$ nm). We subtracted the background fluorescence of free nucleotides on the observed emission peak. DNA substrates were constant at 1 μM, and RecBCD concertation was 1 μM. In the case of ADP binding to RecBCD•dohDNA, the DNA concentration was 8 μM.

mantNucleotide binding curves of the fluorescence change as a function of the free ligand concentration are best fitted by the sum of two Hill plots according to Eq. (4):

$$y = p \cdot \frac{1}{1 + \left(\frac{K_s}{[mN]}\right)^{n_s}} + (1 - p) \cdot \frac{1}{1 + \left(\frac{K_w}{[mN]}\right)^{n_w}} \quad (4)$$

where y is the fraction bound, mN is the ligand concentration, K_s (strong nucleotide states) and K_w (weak nucleotide states) are the equilibrium constants of the first and second phases,

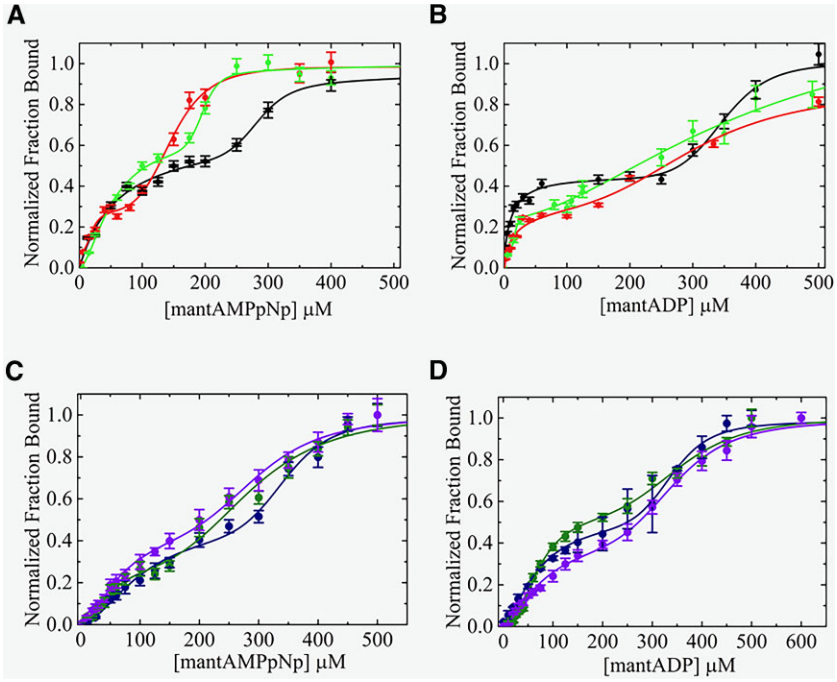

Figure 2. Equilibrium binding of RecBCD and RecBCD × DNA to mantNucleotides. (A, B) Titration curves of mantAMPPpNp (**A**) and mantADP (**B**) binding to RecBCD (•), RecBCD × hpDNA (•) and RecBCD × ssDNA (•). The data for RecBCD × mantAMPPpNp (A) and RecBCD × mantADP (B), collected contemporaneously with the rest of the data, is adapted from (35). (C, D) Titration curves of mantAMPPpNp (**C**) and mantADP (**D**) binding to RecBCD × dohDNA (•), RecBCD × 5ohDNA (•), and RecBCD × 3ohDNA (•). Solid lines show the best fit to Eq. (3). Error bars report the s.e.m. of $n = 3$ independent measurements.

respectively. n_s and n_w are the Hill coefficients of the first and second phases, respectively, and p is the proportionality constant ($0 \leq p \leq 1$). Previously, we showed that the first phase of the binding titration curve reflects binding to the canonical ATP binding sites residing within RecB and RecD. The second phase describes binding to additional weak binding sites. Both are given by macroscopic equilibrium constants K_s and K_w (35).

Stopped-flow measurements

Fluorescence anisotropy real-time dissociation kinetic experiments were performed using a T-format excitation and emission module fitted on an SF-61DX2, TGK Scientific (Bradford on von, UK) stopped-flow apparatus thermostatted at 25 ± 0.1°C. Samples were excited at $\lambda_{ex} = 492$ nm by using vertically polarized light. The emitted vertically and horizontally polarized light was monitored at 90° through a 515 nm long-pass colored glass filter. The G-factor for correction of the differences in gain between the photomultiplier tube detectors was calculated as described by the instrument manufacturer. FA time-resolved transients were analyzed as described previously (38). Equilibrated mixtures of 1:1 complex RecBCD·dohDNA (250 nM) or 1:2 complex RecBCD·ssDNA (RecBCD = 250 nM; 500 nM = ssDNA) in the absence or presence of 1.2 mM Mg·ADP were rapidly mixed with 20 μM unlabeled dohDNA or ssDNA for the dissociation as a function of the nucleotide state. All concentrations are given before mixing. Data were averaged (at least five traces) and analyzed using the Kinetic Studio software provided with the instrument or OriginPro. Time-dependent changes of the fluorescence signal were fitted to the exponential function given in Eq. 5:

$$F(t) = F_\infty + \sum_{i=1}^{n} A_i \cdot e^{-k_i \cdot t} \quad (5)$$

$F(t)$ is the fluorescence signal at time t, F_∞ is the signal at $t_{10\,s}$, A_i is the amplitude, k_i is the observed rate constant, i represents the ith relaxation processes, and n is the total number of relaxation processes.

Results

DNA binding affinities to RecBCD and RecBCD•nucleotide complexes

We used Fluorescence Anisotropy (FA) to measure the equilibrium binding affinity of RecBCD for DNA in the absence and presence of AMPPpNp and ADP. AMPPpNp is a slowly hydrolyzable or non-hydrolyzable ATP analog and can be used to assess the role of binding energy in the transduction process in molecular motors (39).To study various points in the catalytic unwinding reaction cycle, we devised a set of DNA substrates that mimic major biochemical states: binding of RecBCD to a DNA hairpin with a blunt end (hpDNA, Supplementary Figure S1A) simulates the initiation phase; binding to a DNA hairpin with two non-complementary overhangs (dohDNA, Supplementary Figure S1B) represents the DNA fork separation and unwinding; In addition, two substrates with either 5′ or 3′ overhangs (5ohDNA and 3ohDNA, respectively, Supplementary Figure S1C, D) are used to measure the affinity of RecBCD for DNA when only RecB or RecD subunits can access and bind the ssDNA (8,36,40), and a single-stranded DNA substrate (ssDNA,

Supplementary Figure S1E) is used to mimic the translocating complex. All the DNA binding isotherms exhibited hyperbolic dependence curves (Figure 1), enabling us to determine the equilibrium binding constants for the different DNA substrates (Table 1).

ADP modulates the affinity of RecBCD for DNA

The binding of RecBCD to hpDNA, which mimics the initiation step of the catalytic cycle, revealed that the presence and identity of a nucleotide cofactor modulate the complex affinity. Specifically, the ADP bound state showed a ∼3-fold weaker affinity for hpDNA than the APO one, while an intermediate affinity was observed in the presence of AMPpNp (Figure 1, Table 1). The strong affinity of the APO state agrees with earlier results showing the ability of RecBCD to bind and melt blunt-ended duplex DNA in an Mg^{2+}-dependent, ATP-independent manner (40). The differential reduction in RecBCD affinity towards hpDNA in the presence of AMPpNp and ADP states observed may provide a mechanism for RecBCD to initiate translocation from the initial relatively strong binding state to a double-strand DNA site (41).

When we tested the binding of RecBCD to dohDNA, we observed a substantial reduction in the affinity in the presence of ADP (40-fold and 25-fold) compared to the APO and AMPpNp states, respectively; Figure 1B and Table 1). This strong coupling between ADP and dohDNA binding indicates that RecBCD cannot bind strongly simultaneously to both ADP and dohDNA, i.e. the binding of one weakens the affinity of the other and vice versa.

To further dissect the basis for the observed weak binding to dohDNA in the presence of ADP, we characterized two additional DNA substrates containing either a 5ohDNA or 3ohDNA, likely engaging only with RecD or RecB, respectively (Supplementary Figure S1D, E). Generally, RecBCD exhibited a significantly higher affinity towards the asymmetric constructs than for dohDNA (Figure 1B–D and Table 1). Specifically, RecBCD retained a strong affinity towards 5ohDNA and 3ohDNA in the presence of AMPpNp, and RecBCD•ADP displayed an even higher affinity for these DNA constructs. This suggests a weak coupling between the asymmetric substrates and the nucleotide state. We note that the lower FA absolute value observed for the 3ohDNA in the presence of ADP in Figure 1D may be due to a less rigid conformation of the fluorophore at the 3′ overhang than a fluorophore at the 5′ overhang.

The observed differences in the binding affinities of the Apo state of RecBCD towards ssDNA, dohDNA, 5ohDNA, and 3ohDNA suggest that these four complexes interact specifically with their cognate binding sites matching the polarity and orientation of the DNA strands with RecB and RecD polarity (40–42). Hence, RecBCD engages with either 5′ or 3′ overhang DNA strands with a small effect by ADP binding. However, when both overhang DNA are engaged simultaneously with RecBCD (dohDNA substrate), ADP binding strongly weakens RecBCD affinity towards DNA, suggesting communication between RecBCD subunits. On the other hand, in the presence of AMPpNp (Figure 1B-D, Table 1), a less pronounced effect is observed on the binding isotherms between the different substrates. Rather than weakening the binding affinities observed towards dohDNA in the presence of ADP, here, the overall affinity towards dohDNA is approximately the average of the individual binding affinities (34.0 ± 7.0, 31 ± 8, & 166.3 ± 41 nM for RecBCD•AMPpNp*X* dohDNA/5ohDNA/3ohDNA, respectively).

Interaction of RecBCD with ssDNA revealed cooperative binding

We analyzed the binding isotherms of ssDNA to RecBCD with a hyperbolic binding curve assuming no cooperativity (Figure 1E, Eq. (2)). Treating the binding of both ssDNAs with one macroscopic constant showed that none of the nucleotide cofactors affected the affinity of RecBCD towards ssDNA binding (Figure 1E, Table 1). However, since ssDNA binds to RecBCD with a 2:1 stoichiometric ratio (Supplementary Figure S2A), we can also use the Hill equation to approximate the binding isotherm data to determine if RecBCD binds these two ssDNA molecules cooperatively (Figure 1F, Table 1). ssDNA binding to RecBCD without nucleotides shows intermediate cooperativity and a Hill coefficient of n_H ∼1.4, whereas, in the presence of AMPpNp, the cooperativity is slightly negative (n_H ∼ 0.7). Interestingly, while ADP binding weakens the affinity towards ssDNA, it increases the Hill coefficient to n_H ∼2. Hence, when the two DNA binding sites in RecB and RecD are bound to ssDNA, the ADP nucleotide cofactor imposes a different degree of cooperativity, suggesting a different conformation and degree of interaction between RecB and RecD upon the different nucleotide cofactors. This may result from disrupting long-range intramolecular signaling between the three subunits as a response to different nucleotides (43).

Nucleotide-binding to RecBCD and RecBCD•DNA complexes exhibit different degrees of affinities

Having characterized how nucleotides modulate the affinity of RecBCD for different DNA substrates, we turned to characterize how engaging with DNA modulates the affinity of RecBCD for nucleotides. We used FRET between mantNucleotide derivatives and intrinsic tryptophan residues and measured binding at equilibrium (35). We previously showed that the binding of mantNucleotide to RecBCD and RecBCD•DNA complexes displays a biphasic binding isotherm curve to multiple binding sites (35). These macroscopic binding constants describe the two types of nucleotide binding sites: high affinity binding to the catalytic sites (in RecB and RecD) and low affinity binding to 'auxiliary' sites that increase the flux of ATP towards the catalytic sites.

We determined the binding isotherms of ADP and AMPpNp binding to the different RecBCD-DNA complexes. The high-affinity phase displayed a binding constant, K_s, ranging from ∼13 to 106 μM and a Hill coefficient n_s between 0.8 and 3.0 (Table 2). The second weak binding phase constant, K_w, always exhibited a weaker affinity constant, up to three-fold weaker than the weakest strong binding constant measured (K_s = 106 μM compared to K_w = 140 to 350 μM, respectively, Table 2). In addition, these sites showed a comparable higher degree of cooperativity, n_w ranging from 2.5 to 12.0, with significant errors, suggesting that there may be as well a range of cooperative binding induced by different DNA substrates and nucleotide states (Table 2). We identified four RecBCD•DNA biochemical intermediates that differentially affected nucleotide binding, producing RecBCD•DNA•nucleotide complexes with different affinities (Table 2).

Table 2. Equilibrium constants for strong nucleotide binding sites to RecBCD and RecBCD·DNA complexes

Equilibrium Constant	Complex structure	Nucleotide analog binding	K_s(μM)	Complex annotation	n_s	$\Delta G_s°'$ (kJ·mol^{-1})
$^4K_{mA}$		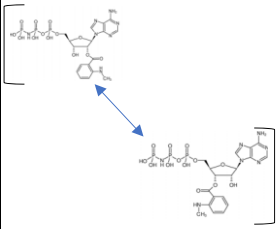	52.4 ± 7.8	RecBCD·mA	0.99 ± 0.1	-24.4 ± 0.4
$K_{mA,\ hp}$	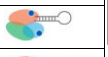		73.5 ± 9.3	RecBCD·hpDNA·mA	1.44 ± 0.3	-23.6 ± 0.3
$K_{mA,\ doh}$	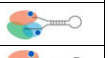		106.0 ± 33.5	RecBCD·dohDNA·mA	1.8 ± 0.4	-22.7 ± 0.8
$K_{mA,5oh}$	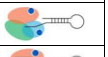		47.8 ± 22.1	RecBCD·5ohDNA·mA	2.0 ± 1.0	-24.6 ± 1.1
$K_{mA,3oh}$	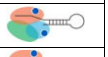		71.0 ± 28.3	RecBCD·3ohDNA·mA	1.7 ± 0.4	-23.7 ± 1.0
$K_{mA\ ss}$			20.0 ± 5.9	RecBCD·ssDNA·mA	2.90 ± 0.9	-26.8 ± 0.7
$^4K_{mD}$		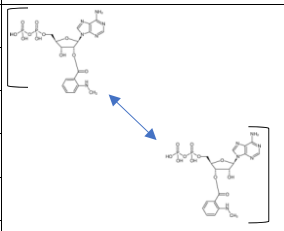	13.2 ± 3.1	RecBCD·mD	0.95 ± 0.1	-27.8 ± 0.6
$K_{mD,\ hp}$	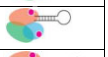		29.2 ± 11.8	RecBCD·hpDNA·mD	0.81 ± 0.2	-25.9 ± 1.0
$K_{mD,\ doh}$	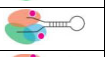		70.9 ± 19.4	RecBCD·dohDNA·mD	1.5 ± 0.3	-23.7 ± 0.7
$K_{mD,5oh}$			70.5 ± 8.6	RecBCD·5ohDNA·mD	2.4 ± 0.4	-23.7 ± 0.3
$K_{mD,3oh}$			80.8 ± 25.8	RecBCD·3ohDNA·mD	1.5 ± 0.3	-23.3 ± 0.8
$K_{mD,\ ss}$			15.7 ± 3	RecBCD·ssDNA·mD	2.85 ± 1.7	-27.4 ± 0.5

1. mantAMP-pNp (mA):2′/3′-*O*-(*N*-Methyl-anthraniloyl)-adenosine-5′-[(β, γ)-imido]-triphosphate mantADP (mD): 2′/3′-*O*-(*N*-M2′/3′-*O*-(*N*-methyl-anthraniloyl)-adenosine-5′-diphosphate,
2. Fitted parameters for the sum of two Hills equations, K_s are the equilibrium dissociation constants for nucleotides association to the strong binding sites; n_s is the Hill coefficient for nucleotides' association of the strong binding sites
3. $\Delta G_s°' = RTln(K_s)$ is the standard binding energies at 1 M ligand, R is the gas constant (8.314 J mol^{-1} K^{-1}), $T = 298.15$°K for the strong binding sites, respectively.
4. Previously reported (48).
RecB, RecC and RecD are shown as oval shapes in orange, green, and light blue, respectively; ATP and ADP are drawn as spheres in blue and red, respectively.

AMPpNp binds to the strong binding sites in the RecBCD•dohDNA complex with two-fold weaker affinity than RecBCD ($K_{mA,doh} = 106 \pm 33.5$ versus $K_{mA} = 52.4 \pm 7.8$, respectively, Figure 2, Table 2). In contrast, the affinities towards RecBCD•5ohDNA and RecBCD•3ohDNA ($K_{mA,5oh} = 47.8 \pm 22.1$ and $K_{mA,3oh}$ 71.0 ± 28.3 respectively, Figure 2A–D, Table 2) are comparable to the one for RecBCD. These observations further suggest that the coupling between the DNA and nucleotide binding sites is more pronounced when both DNA binding sites are occupied.

Two parameters are revealed by the binding of ADP towards RecBCD•DNA complexes. First, the overall affinity towards ADP is weakened in all substrates examined as compared to RecBCD ($K_{mD,doh} = 70.9 \pm 19.4$, $K_{mD,5oh} = 70.5 \pm 8.6$, $K_{mD,3oh} = 80.8 \pm 25.8$ and $K_{mD} = 13.2 \pm 3.1$, respectively, Figure 2, Table 2). Next, when the DNA substrates are physically connected ahead of the binding sites, there seems to be a more substantial impact on the nucleotide-binding affinities towards the strong binding sites. Therefore, it may well be that tension in the closed DNA substrates upstream from RecBCD•DNA sites has a more substantial effect on intersubunit communication. Overall, ADP binding to RecBCD•DNA complexes is more effective than AMPpNp binding in modulating the RecBCD•DNA strong binding state, weakening the interaction with DNA in the presence of ADP. In contrast to the modulation of nucleotide binding to the catalytic sites by engaging DNA, the affinity for the auxiliary sites shows no significant change between the RecBCD•DNA states of RecBCD and in the absence of any DNA substrates (Supplementary Table S2). These results suggest that the weaker nucleotide binding sites (auxiliary sites) are uncoupled to nucleotide binding to the strong binding sites and are unaffected by DNA binding.

Thermodynamic coupling constants between the DNA and nucleotide binding states reveal binding linkage within the RecBCD•DNA•nucleotide complex

The free energy derived from the binding constants of the RecBCD•DNA•nucleotide complex formation permits quantifying the degree of *linkage* and the thermodynamic coupling constant (TC) between any four states within a closed reaction cycle (44). Importantly, this analysis can provide the degree of coupling between the different states, primarily when a cofactor modulates the affinity towards a substrate or a substrate modulates the affinity towards the cofactor. In addition, it provides an estimation of the intrinsic consistency of a set of measurements, as the overall change in free energy $\Delta G°$ for a closed reaction cycle should be balanced, i.e. $\Delta G° = 0$. Therefore, the TC equilibrium constant pairs within a balanced thermodynamic coupling constant should be equal, i.e. $K_{mA,hp}/K_{mA}$ and $K_{hp,mA}/K_{hp}$. Thus, ratios significantly >1 report stronger coupling between the measured states, whereas ratios ∼ 1 report weak coupling, i.e. indicate that nucleotide binding does not affect the affinity of RecBCD towards DNA and *vice versa*. Supplementary Figure S3 shows the ten closed reaction cycles corresponding to our five DNA substrates and two nucleotide state measurements. The results of TC analysis for the cycles of hpDNA, dohDNA, 5ohDNA, 3ohDNA and ssDNA, in the absence or presence of either AMPpNp or ADP, are summarized in Table 3. The detailed thermodynamic squares are balanced for all the AMPpNp states and two states of ADP binding to RecBCD•hpDNA and RecBCD•ssDNA (Table 4 and Supplementary Figure S3). AMPpNp seems to possess weak coupling with RecBCD; hence, RecBCD can bind both the AMPpNp nucleotide and DNA quite

Table 3. Thermodynamic coupling parameters associated with RecBCD, RecBCD × DNA, RecBCD × DNA × nucleotide complexes

Thermodynamic square	Thermodynamic coupling parameter	[1]Thermodynamic coupling constant	[2]Detailed thermodynamic balance of RecBCD ligated states.
A, hp	$K_{mA,\,hp}/K_{mA}$	1.4	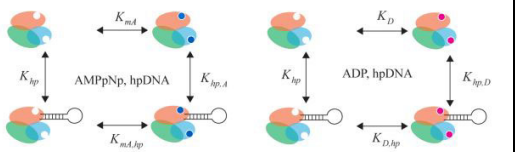
	$K_{hp,\,A}/K_{hp}$	2	
D, hp	$K_{D,\,hp}/K_{D}$	2.2	
	$K_{hp,\,D}/K_{hp}$	3	
A, doh	$K_{mA,\,doh}/K_{mA}$	2	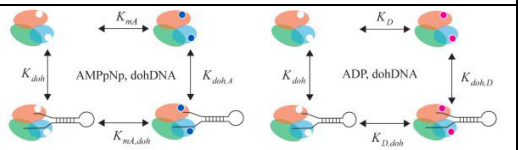
	$K_{doh,\,A}/K_{doh}$	1.8	
D, doh	$K_{mD,\,doh}/K_{D}$	5.4	
	$K_{doh,\,D}/K_{doh}$	42.9	
A, 5oh	$K_{mA,\,5oh}/K_{mA}$	0.9	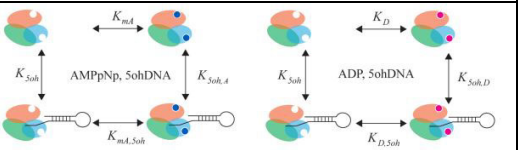
	$K_{5oh,\,A}/K_{5oh}$	1	
D, 5oh	$K_{D,5oh}/K_{D}$	5.3	
	$K_{5oh,\,D}/K_{5oh}$	0.3	
A, 3oh	$K_{mA,3oh}/K_{mA}$	1.4	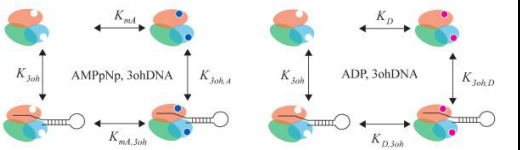
	$K_{3oh,\,A}/K_{3oh}$	1.8	
D, 3oh	$K_{D,3oh}/K_{D}$	6.1	
	$K_{3oh,\,D}/K_{3oh}$	0.2	
A, ss	$K_{mA,\,ss}/K_{mA}$	0.4	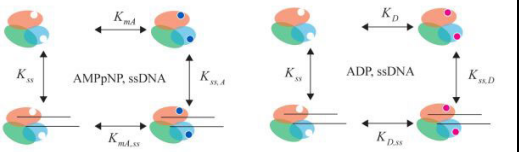
	$K_{ss,\,A}/K_{ss}$	0.6	
D, ss	$K_{mD,\,ss}/K_{D}$	1.2	
	$K_{ss,\,D}/K_{ss}$	1.9	

[1]Calculated from the detailed thermodynamic squares in the right column.
[2]The schemes describe the ligated states of the initiation complex (first row, hpDNA, stoichiometry 1:1), and unwinding complex (second row, dohDNA, stoichiometry 1:1). The boxes in the third and fourth rows are asymmetric substrates engaged either with RecD (5ohDNA) or RecB (3ohDNA), and the translocation complex (fifth row, ssDNA, stoichiometry 1:2). The equilibrium constants, and hence the nucleotides binding occupancy in the model, correspond only to the strong nucleotide binding sites. The equilibrium constants and the free energy calculated (Tables 1 and 2) are the detailed balance thermodynamic squares shown in the reaction schemes. H – RecBCD, hp – hpDNA, doh – dohDNA, 5oh – 5ohDNA, 3oh – 3ohDNA, ss – ssDNA, A – AMPpNp, D – ADP, mA – mantAMPpNp, mD – mantADP. RecB, RecC, and RecD are shown as oval shapes in orange, green, and light blue, respectively; A/mA are shown as •, and D/mD are shown as • in RecBCD canonical nucleotide binding sites. The DNA substrates are shown in each RecBCD complex as black lines.

strongly simultaneously. AMPpNp presumably mimics either the pre-hydrolysis-bound ATP or the post-hydrolysis state ADP•Pi state, suggesting that RecBCD can remain strongly bound to the DNA during these states. However, ADP shows stronger coupling in the hpDNA and, to some extent, in the ssDNA. This suggests that these weaker binding states for ADP may be more dissociative biochemical intermediates when the ADP state is mainly populated during the ATPase cycle of RecBCD. Finally, for three thermodynamics squares: $(K_{D,doh}/K_D)/(K_{doh,D}/K_{doh})$, $(K_{D,5oh}/K_D)/(K_{5oh,D}/K_{5oh})$ and $(K_{D,3oh}/K_D)/(K_{3oh,D}/K_{3oh})$ (Figure S3, marked within yellow) the calculated ratios between the TC pairs are ∼0.13, ∼18 and ∼30, respectively. This suggests an unbalanced close reaction cycle with these three DNA substrates. Two factors may contribute to this: First, ADP binding is measured from the reverse pathway of the ATPase cycle, so it may not necessarily represent the same state after Pi's release. In the kinetic scheme, ADP is bound when the ATPase cycle proceeds via a productive ATP hydrolysis forward pathway (45). Hence, a structural ADP state could not be accessible from the reverse binding of ADP to RecBCD. In addition, our model for nucleotide binding is based on mantNucleotides, which may result in different affinity than unmodified nucleotides.

Table 4. Dissociation kinetics of DNA from RecBCD·dohDNA and RecBCD·dohDNA·ADP

Kinetic reaction	$k_{obs,fast}$ (s^{-1})	$k_{obs,slow}$ (s^{-1})
RecBCD·dohDNA* versus hpDNA	14.2 ± 0.3	0.4 ± 0.004
RecBCD·dohDNA*·ADP versus hpDNA	33.7 ± 0.5	2.2 ± 0.03
RecBCD·dohDNA* *ss*DNA	19.7 ± 0.4	1.0 ± 0.01
RecBCD·dohDNA*·ADP versus ssDNA	47.4 ± 0.7	1.3 ± 0.03

dohDNA* is the labeled species of DNA with FAM(6-fluorescein amidite).

RecB^{K29Q}CD mutant affects the degree of TC between DNA and nucleotide binding

Ideally, measuring the TC separately for RecB and RecD may increase the quantitative resolution of the DNA and nucleotide communication. However, the absence of intersubunit communication may diminish and exhibit a less dramatic TC effect. We have utilized a nucleotide binding and catalytically deficient mutant in the RecB subunit, RecB^{K29Q}CD, previously characterized (35), to assess if the nucleotide canonical binding site in RecB may affect the TC utilizing the different DNA substrates and if the RecD WT subunit within this construct retains the nucleotide-binding linkage. RecB^{K29Q}CD binding to dohDNA and the 5ohDNA binding in the absence or presence of ADP show strong coupling as both substrates engage with the RecD unmutated subunit. The weakening in the presence of ADP was ∼10-fold and ∼7-fold for dohDNA and 5ohDNA, respectively (Supplementary Figure S3, Supplementary Table S3). Remarkably, the binding isotherms of 3ohDNA to RecB^{K29Q}CD in the absence or presence of ADP are comparable. The 3ohDNA interacts with the RecB subunit. The mutation in the nucleotide-binding site makes it less prone to communicate the nucleotide state as in the RecBCD WT and supports the ADP as the weak binding state.

ADP bound to RecBCD•DNA complex accelerates the kinetics of DNA dissociation

dohDNA bound to RecBCD in the presence of ADP exhibits reduced affinity compared to when ADP is absent. In addition, dohDNA shows the strongest modulation of binding to RecBCD in the presence of any other DNA substrates we have examined in the presence of ADP. Previously, we determined the kinetics of nucleotide binding to RecBCD, which can only be measured at 6°C due to the rapid kinetics of RecBCD (35). The nucleotide dissociation could not be determined even at low temperatures in conventional stopped-flow, suggesting rate constants of nucleotide dissociation faster than 1000 s^{-1}, which correlates with the high ATPase cycle and velocity of DNA unwinding by RecBCD. Therefore, we set to measure whether DNA dissociation can be determined using time-resolved FA kinetics. Specifically, ADP, in addition to its effectiveness as modulating the equilibrium constant of dohDNA towards RecBCD, may also affect the dissociation rate of dohDNA, suggesting an indirect contribution to the weaker affinity observed.

Mixing pre-formed RecBCD•dohDNA rapidly with AMPpNp shows no dissociation while mixing rapidly with ADP shows some rapid dissociation followed by slow decay (Figure 4A). In contrast, when rapidly mixing with ATP, we observed exponential decay to nearly complete dissociation of the fluorescently labeled DNA. This suggests that with the cycling of ATP hydrolysis, RecBCD translocates, followed by the subsequent dissociation of the unwound dohDNA from RecBCD as observed by the decrease in FA (Figure 4A). Therefore, we wanted to closely examine if the dissociation of DNA RecBCD•dohDNA•ADP is enhanced as compared to the absence of ADP. RecBCD•dohDNA or RecBCD•dohDNA•ADP was rapidly mixed with unlabeled DNA (hpDNA or ssDNA), and its dissociation followed the decrease in FA (Figure 4B). Table 4 summarized the observed rate constant of dohDNA dissociation kinetics. The rates show an apparent enhancement of DNA dissociation with two exciting observations. The RecBCD•dohDNA•ADP complex exchanges DNA faster than RecBCD•dohDNA, suggesting that the ADP bound state is not only thermodynamically weaker but also kinetically can the bound DNA dissociates more quickly in the presence of ADP. The other important observation is that ssDNA exchange better or competes faster than hpDNA to both complexes in the absence or presence of ADP. Overall, the presence of ADP in the RecBCD-dohDNA complexes enhances dohDNA dissociation in both cases of hpDNA and ssDNA as competitive substrates by more than two-fold in both cases (Figure 4B, Table 4). This further strengthens the observation dissociation, whether momentarily or with the complex, modulated in RecBCD despite its high unwinding velocity and tight DNA binding cavities.

Discussion

In this work, we have studied quantitatively the degree of coupling between DNA substrates mimicking unwinding intermediates and nucleotide states in RecBCD. Our results demonstrate that nucleotide coupling exists in RecBCD and is significant enough to enable the energetic landscape to allow differential binding of RecBCD to its DNA track, as seen in other molecular motors. This observed differential binding is associated with a stepping mechanism of molecular motors during high translocation. Additional parameters, such as unidirectional movement and kinetic constant for translocation >1 (i.e. $k_{forward}/k_{dissociation} > 1$), are requisite. ADP binding induces the strongest coupling compared to the APO or AMPpNp bound states. All three substrates, dohDNA, 5ohDNA, and 3ohDNA, affect ADP binding, unlike AMPpNp. When RecBCD is bound to ADP, we observed the most robust modulation in the binding affinity to all the substrates compared to the APO and AMPpNp states.

Furthermore, our results support that the occupancy of both RecB and RecD with bound ssDNA, simultaneously is essential for RecBCD intersubunit communication. Two significant observations support this requirement. First, the hpDNA substrate, which lacks ssDNA overhangs long enough to interact fully with RecB and RecD, does not show such an coupling effect. Therefore, both ssDNAs beyond the fork must be strongly embedded within their binding sites to impose communication between nucleotide and DNA binding. The second observation stems from the binding affinity towards dohDNA, compared to that for either 5ohDNA or 3ohDNA. The 5ohDNA binds well in the presence of ADP; however, when ssDNA overhangs are present in both antiparallel strands, ADP has the opposite effect inducing weak binding towards dohDNA. The observation that single-stranded overhang substrates do not have the same impact on ADP binding to RecBCD implies that intersubunit communication

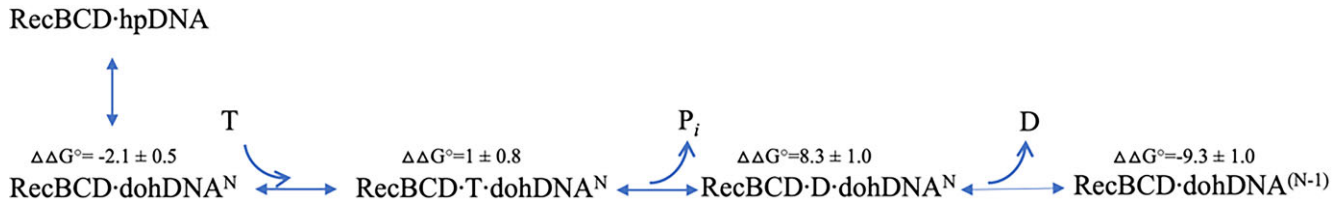

Figure 3. Biochemical intermediates along a discrete model for unwinding from state N (i.e. N bp unwound) to state N-1. The model assumes one ATP molecule is hydrolyzed per bp unwound. For each complex, $\Delta\Delta G^\circ$ is calculated at saturating nucleotide concentration from the change in $\Delta G^\circ{}'_{association}$ of the two complex-forming reactions. All $\Delta\Delta G^\circ$ are reported in kJ mol^{-1} (Table 1).

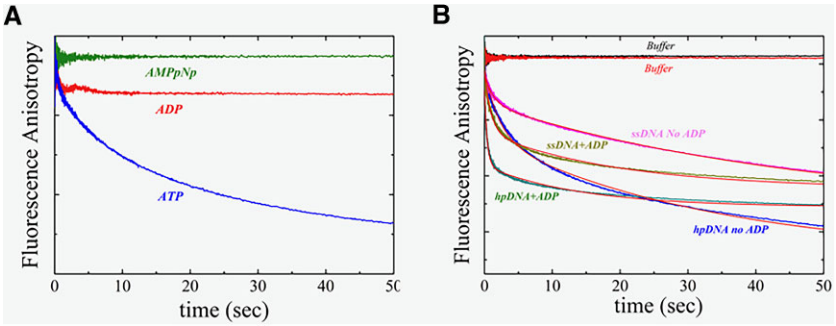

Figure 4. Kinetics of DNA substrates dissociation from RecBCD followed by real-time FA. (**A**) RecBCD·dohDNA (250 nM final concentrations) was rapidly mixed with 2 mM AMPpNp (green), ADP (red), or ATP (blue), and the DNA dissociation was followed by a decrease in FA. Traces shown are an average of 5 traces each. (**B**) RecBCD·dohDNA or RecBCD·dohDNA·ADP (250 nM) and [ADP] at 2 mM were rapidly mixed with buffer or with 20 μM unlabeled DNA substrates. Controls are shown for the complex without and with ADP bound vs buffer (black & red traces, respectively), RecBCD·dohDNA vs ssDNA (pink) and hpDNA (blue), and RecBCD·dohDNA·ADP vs ssDNA (gold) and hpDNA (green). Traces shown are an average of three shots each. The black lines through the data best fit the double exponential equation (Table 4).

between RecBCD subunits is induced to a fuller extent when both RecB and RecD are bound to ssDNA (8,35,41,46).

In our current work, we have extended our previous analysis of nucleotide binding to RecBCD in the presence of DNA substrates and performed a detailed analysis of the sum of two hill plots based on our previous solution of the binding isotherms for RecBCD (35). Importantly, we observed that different DNA substrates affect both parameters of the strong (K_s) and weak binding constant K_w. Straightforwardly, this suggests that long-range interactions also affect the weak binding state beyond the immediate effect on the DNA affinities as a function of the nucleotide state and vice-versa. In previous studies, we proposed a deterministic model that the auxiliary ATP binding sites (weak binding sites, primarily located on RecC) serve as a reservoir for ATP to increase funneling into the active sites. The observation that their affinities change as a function of DNA substrates suggests that long-range interactions also affect the dynamic of RecBCD auxiliary ATP binding sites by modulating their affinities. This, in turn, may impact the efficiency of RecBCD as a robust and processive DNA helicase.

Further evidence for the importance of occupancy of both RecB and RecD to propagate the observed TC is evident by the 3′ overhang DNA. In this case, the 3ohDNA substrate displays weaker affinity towards RecBCD in the absence or presence of AMPpNp than when ADP is bound. This suggests that AMPpNp may generate a weak binding state when one DNA binding site is occupied. Hence, ADP is not the sole cofactor to weaken DNA binding. However, the TC for these states, $K_{mA,3oh}/K_{mA}$ and $K_{3oh,\,mA}/K_{3oh}$, is very weakly coupled, and the detailed balance is consistent with the thermodynamic cycle among these states. Corollary, there may be a weakening in the affinity among the abovementioned states, but they don't trigger the strong coupling effects observed with ADP in the presence of dohDNA. Furthermore, when both subunits are engaged with ssDNA, the observed TC is most likely indicative of interacting residues residing remotely from the DNA binding sites within RecB and RecD (41).

Characterization of the major biochemical intermediates along the reaction coordinates of RecBCD allows us to formulate a minimal energetic model for the unwinding of a single ATP hydrolysis cycle (Figure 3). The calculated overall $\Delta\Delta G^\circ$ from RecBCD•dohDNA^N to RecBCD•dohDNA^{N-1} (i.e. the $\Delta\Delta G^\circ$ associated with unwinding and translocating 1 bp) is about ∼7 kJ mol^{-1} which is about one quarter the energy released from the hydrolysis of one mole of ATP. Assuming that the ATPase cycles of RecB and RecD are unsynchronized and possess different nucleotide states during ATPase cycling, the overall $\Delta\Delta G^\circ$ would be an average of two distinct states at any given moment during the unwinding. This will minimize the transition barrier between states. For example, Pi release seems to be an unfavorable intermediate as the $\Delta\Delta G^\circ = +8.3 \pm 1.0$. However, ADP release is highly favorable $\Delta\Delta G^\circ = -9.3 \pm 1.0$. Hence, if, i.e. RecB releases Pi and RecD releases ADP, the net change is negative, $\sim\Delta\Delta\Delta G^\circ = -1.0$, enabling RecBCD as complex to overcome unfavorable transition states. We proposed that this strategy by RecBCD will allow it to progress with minimum energy barriers as a holoenzyme.

Our model proposes that RecB and RecD switch between strong and weak binding states with a degree of synchronization during translocation and unwinding that needs to be consistent with previous observations. RecB and RecD possess different translocation and unwinding rates, which impose

asynchronous rates of unwinding and translocation (pre-Chi sequences), and RecB has two translocation activities, primary with 3′ to 5′ polarity and 5′ to 3′secodnary (16,47,48). It may well be that the 5′ to 3′ translocation activity by RecB during the pre-Chi is assisting the translocase activity of RecD. Hence, this activity results in a faster RecD activity, as suggested (16). Furthermore, Lohman and coworkers suggest that the secondary RecBC ssDNA translocase activity is insensitive to the ssDNA backbone polarity (36,48). A plausible mechanism could be threading the ssDNA ahead of RecD during pre-chi translocation. Hence, we proposed that this domain can be tethered by very weak electrostatic interaction with the 5′–3′ DNA backbone, making it much less sensitive to the nucleotide state far from the primary translocase activity of RecB (48). RecBCD translocates and unwinds as a unit, i.e. it remains a heterodimer during all states, off or on the DNA and with all nucleotides. A plausible explanation for the apparent differences in the unwinding rates between individual subunits versus those within the holoenzyme is inherently encoded by crosstalk and regulation between RecBCD subunits. The minor differences in translocation rates of RecB and RecD are most likely to be tolerated during unwinding *in vivo* until an encounter with chi-sequence, making it with much less impact on the robust processivity of RecBCD (16,36,47,48). We cannot exclude that forces and viscosity impounding the motors during reaction under physiological conditions will equilibrate the rates observed *in vitro*.

Models for the unwinding mechanism were proposed based on crystallographic studies of biochemical intermediates for UvrD, PcrA, and RecBCD DNA helicases of SF1 (49–51). UvrD, model as a monomer unwinds by a two-part power stroke termed wrench-and-inchworm mechanism. The rotational angle and translational distance of DNA achieved by this cycle of conformational changes by UvrD is 1 bp per ATP hydrolyzed (50). PcrA seems to have evolved with a mechanism of base filliping of the duplex DNA, and separation of 1 bp occurs per ATP hydrolyzed. In both cases, domain movement or array of amino-acids filliping coupled to domain swiveling are biochemical transitions that will limit the velocity of unwinding by 2–3 orders of magnitude in comparison to RecBCD unwinding observed unwinding rates (16,52) and indeed UvrD and PcrA are much slower DNA helicases than RecBCD (53–56). Bianco and Kowalczykowski (57) have proposed a similar stepping mechanism for RecBC where RecB contains two DNA binding domains that create a leading and a trailing head during unwinding. Such a mechanism is consistent with our idea; however, the energetics and the time duration of the different complexes are required to model strong and weak binding states.

It remains to be shown if within RecBCD, smaller-scale conformational changes occur during processive unwinding, as observed in UvrD and PcrA. RecBCD translocation and unwinding can be view as before and after chi recognition sequence and may shed some light on its unwinding mechanism. CryoEM of RecBCD with DNA containing a Chi sequence compared to RecBCD containing a non-Chi DNA sequence argues that significant changes are induced upon the Chi DNA sequence within the RecC subunit (32). Significant conformational changes have also recently been reported in the RecB nuclease domain upon Chi sequence recognition without distorting the RecBCD inter-subunit interactions using elegant complementation assay in trans of the RecB nuclease domain (58). It is further confirmed that losing the RecB nuclease domain substantially impacts RecBCD translocation unwinding rates of RecBCD (59). Corollary, this may suggest that RecBCD does not undergo substantial conformational changes ahead of the Chi sequence, translocating with a minimum energy barrier along the reaction pathway.

The RecB ‘arm’ at the forefront makes extensive contact with the fork created upon dsDNA binding and passive DNA melting (41). Additional contacts of the junction of the dsDNA with the ‘pin’ domain of RecC add to the overall RecBCD-DNA interaction. RecB 2A subdomain interacts with the 3′ overhang ssDNA, while RecD subdomains 1A and 2A interact with the 5′ overhang ssDNA. During the translocation of RecB and RecD motors in opposite polarity, the contacts of both subunits with DNA dynamically change to allow movement. Such dynamics are driven by different nucleotide binding ligated states, modulating the affinity as resolved in this work. Strong binding states can be viewed as the ‘pulling’ states, while the weak binding states are the ‘relieving’ states, allowing for productive advancement of the RecBCD motor, alternating these events between RecB and RecD. Notably, to result in processive translocation, the weak binding states (or strong binding states) cannot coexist in both subunits simultaneously. Hence, allosteric communications likely exist and involve interactions across all the DNA contact sites throughout the three RecBCD subunits.

Data availability

The authors confirm that the data supporting the findings of this study are available within the article and Supplementary Data.

Supplementary data

Supplementary Data are available at NAR Online.

Acknowledgements

We thank Dr Stephen C. Kowalczykowski and Dr Theetha Pavankumar for the RecBCD expression system and their assistance in the RecBCD purification protocol (the University of California, Davis, California).

Funding

Israel Science Foundation [296/13, 712/18 to A.H., 1902/12, 937/20 to A.K.]; Marie Curie Career Integration Award [1403705/11 to A.H., 293923/11 to A.K.]. Funding for open access charge: Israel Science Foundation [712/18 to AH].

Conflict of interest statement

None declared.

References

1. Brosh,R.M. (2013) DNA helicases involved in DNA repair and their roles in cancer. *Nat. Rev. Cancer*, **13**, 542–558.
2. Yeeles,J.T.P. and Dillingham,M.S. (2010) The processing of double-stranded DNA breaks for recombinational repair by helicase–nuclease complexes. *DNA Repair (Amst.)*, **9**, 276–285.
3. Smith,G.R. (2012) How RecBCD Enzyme and Chi Promote DNA Break Repair and Recombination: A Molecular Biologist’s View. *Microbiol. Mol. Biol. Rev.*, **76**, 217–228.

4. Liu,B., Baskin,R.J. and Kowalczykowski,S.C. (2013) DNA unwinding heterogeneity by RecBCD results from static molecules able to equilibrate. *Nature*, **500**, 482–485.
5. Boehmer,P.E. and Emmerson,P.T. (1992) The RecB subunit of the *Escherichia coli* RecBCD enzyme couples ATP hydrolysis to DNA unwinding. *J. Biol. Chem.*, **267**, 4981–4987.
6. Dillingham,M.S., Spies,M. and Kowalczykowski,S.C. (2003) *RecBCD enzyme is a bipolar DNA helicase*, **423**, 893–897.
7. Masterson,C., Boehmer,P.E., McDonald,F., Chaudhuri,S., Hickson,I.D. and Emmerson,P.T. (1992) Reconstitution of the activities of the RecBCD holoenzyme of *Escherichia coli* from the purified subunits. *J. Biol. Chem.*, **267**, 13564–13572.
8. Singleton,M.R., Dillingham,M.S., Gaudier,M., Kowalczykowski,S.C. and Wigley,D.B. (2004) Crystal structure of RecBCD enzyme reveals a machine for processing DNA breaks. *Nature*, **432**, 187–193.
9. Wigley,D., Singleton,M., Dillingham,M., Gaudier,M. and Kowalczykowski,S. (2005) Crystal structure of RecBCD : A machine for processing DNA breaks. *GBM Annual Spring Meeting Mosbach 2005*, **2005**, 187–193.
10. Taylor,A.F. and Smith,G.R. (1995) Monomeric RecBCD enzyme binds and unwinds DNA. *J. Biol. Chem.*, **270**, 24451–24458.
11. Spies,M., Amitani,I., Baskin,R.J. and Kowalczykowski,S.C. (2007) RecBCD enzyme switches lead motor subunits in response to χ recognition. *Cell*, **131**, 694–705.
12. Taylor,A.F. and Smith,G.R. (2003) RecBCD enzyme is a DNA helicase with fast and slow motors of opposite polarity. *Nature*, **423**, 889–893.
13. Finkelstein,I.J., Visnapuu,M.L. and Greene,E.C. (2010) Single-molecule imaging reveals mechanisms of protein disruption by a DNA translocase. *Nature*, **468**, 983–987.
14. Terakawa,T., Redding,S., Silverstein,T.D. and Greene,E.C. (2017) Sequential eviction of crowded nucleoprotein complexes by the exonuclease RecBCD molecular motor. *Proc. Natl. Acad. Sci. U.S.A.*, **114**, E6322–E6331.
15. Patel,S.S. and Donmez,I. (2006) Mechanisms of helicases. *J. Biol. Chem.*, **281**, 18265–18268.
16. Xie,F., Wu,C.G., Weiland,E. and Lohman,T.M. (2013) Asymmetric regulation of bipolar single-stranded DNA translocation by the two motors within *Escherichia coli* RecBCD helicase. *J. Biol. Chem.*, **288**, 1055–1064.
17. Wong,I. and Lohman,T.M. (1992) Allosteric effects of nucleotide cofactors on *Escherichia coli* Rep helicase-DNA binding. *Science*, **256**, 350–355.
18. Olivares,A.O. and De La Cruz,E.M. (2005) Holding the reins on myosin V. *Proc. Natl. Acad. Sci. U.S.A.*, **102**, 13719–13720.
19. Wang,Q. and Kolomeisky,A.B. (2019) Theoretical analysis of run length distributions for coupled motor proteins. *J. Phys. Chem. B*, **123**, 5805–5813.
20. Zhang,Y. and Kolomeisky,A.B. (2018) Theoretical investigation of distributions of run lengths for biological molecular motors. *J. Phys. Chem. B*, **122**, 3272–3279.
21. Stukalin,E.B., Phillips,H. and Kolomeisky,A.B. (2005) Coupling of two motor proteins: a new motor can move faster. *Phys. Rev. Lett.*, **94**, 238101.
22. Von Hippel,P.H. (2004) Helicases become mechanistically simpler and functionally more complex. *Nat. Struct. Mol. Biol.*, **11**, 494–496.
23. Hackney,D.D. (1996) The kinetic cycles of myosin, kinesin, and dynein. *Annu. Rev. Physiol.*, **58**, 731–750.
24. Lohman,T.M., Thorn,K. and Vale,R.D. (1998) Staying on track: common features of DNA helicases and microtubule motors. *Cell*, **93**, 9–12.
25. Lohman,T.M., Tomko,E.J. and Wu,C.G. (2008) Non-hexameric DNA helicases and translocases: Aechanisms and regulation. *Nat. Rev. Mol. Cell Biol.*, **9**, 391–401.
26. Henn,A., Bradley,M.J.M.J. and De La Cruz,E.M.E.M. (2012) ATP utilization and RNA conformational rearrangement by DEAD-box proteins. *Annu. Rev. Biophys.*, **41**, 247–267.
27. Henn,A. and Sadot,E. (2014) The unique enzymatic and mechanistic properties of plant myosins. *Curr. Opin. Plant Biol.*, **22**, 65–70.
28. Adler,N.S., Cababie,L.A., Sarto,C., Cavasotto,C.N., Gebhard,L.G., Estrin,D.A., Gamarnik,A.V., Arrar,M. and Kaufman,S.B. (2022) Insights into the product release mechanism of dengue virus NS3 helicase. *Nucleic Acids Res.*, **50**, 6968–6979.
29. Amundsen,S.K. and Smith,G.R. (2023) RecBCD enzyme: mechanistic insights from mutants of a complex helicase-nuclease. *Microbiol. Mol. Biol. Rev.*, **87**, e00041-23.
30. Ganesan,S. and Smith,G.R. (1993) Strand-specific binding to duplex DNA ends by the subunits of the Escherichia coli RecBCD enzyme. *J. Mol. Biol.*, **229**, 67–78.
31. Farah,J.A. and Smith,G.R. (1997) The RecBCD enzyme initiation complex for DNA unwinding: enzyme positioning and DNA opening. *J. Mol. Biol.*, **272**, 699–715.
32. Cheng,K., Wilkinson,M., Chaban,Y. and Wigley,D.B. (2020) A conformational switch in response to Chi converts RecBCD from phage destruction to DNA repair. *Nat. Struct. Mol. Biol.*, **27**, 71–77.
33. Roman,L.J. and Kowalczykowski,S.C. (1989) Characterization of the helicase activity of the *Escherichia coli* RecBCD enzyme using a novel helicase assay. *Biochemistry*, **28**, 2863–2873.
34. Roman,L.J. and Kowalczykowski,S.C. (1989) Characterization of the adenosinetriphosphatase activity of the *Escherichia coli* RecBCD enzyme: relationship of ATP hydrolysis to the unwinding of duplex DNA. *Biochemistry*, **28**, 2873–2881.
35. Zananiri,R., Mangapuram Venkata,S., Gaydar,V., Yahalom,D., Malik,O., Rudnizky,S., Kleifeld,O., Kaplan,A. and Henn,A. (2022) Auxiliary ATP binding sites support DNA unwinding by RecBCD. *Nat. Commun.*, **13**, 1806.
36. Wu,C.G., Bradford,C. and Lohman,T.M. (2010) *Escherichia coli* RecBC helicase has two translocase activities controlled by a single ATPase motor. *Nat. Struct. Mol. Biol.*, **17**, 1210–1217.
37. Otto,M.R., Lillo,M.P. and Beechem,J.M. (1994) Resolution of multiphasic reactions by the combination of fluorescence total-intensity and anisotropy stopped-flow kinetic experiments. *Biophys. J.*, **67**, 2511–2521.
38. Henn,A., Cao,W., Licciardello,N., Heitkamp,S.E., Hackney,D.D. and De La Cruz,E.M. (2010) Pathway of ATP utilization and duplex rRNA unwinding by the DEAD-box helicase, DbpA. *Proc. Natl. Acad. Sci. U.S.A.*, **107**, 4046–4050.
39. Bagshaw,C. (2001) ATP analogues at a glance. *J. Cell Sci.*, **114**, 459–460.
40. Wong,C.J. and Lohman,T.M. (2008) Kinetic control of Mg^{2+}-dependent melting of duplex DNA ends by Escherichia coli RecBC. *J. Mol. Biol.*, **378**, 761–777.
41. Hao,L., Zhang,R. and Lohman,T.M. (2021) Heterogeneity in *E. coli* RecBCD helicase-DNA binding and base pair melting. *J. Mol. Biol.*, **433**, 167147.
42. Wu,C.G. and Lohman,T.M. (2008) Influence of DNA end structure on the mechanism of initiation of DNA unwinding by the *Escherichia coli* RecBCD and RecBC helicases. *J. Mol. Biol.*, **382**, 312–326.
43. Amundsen,S.K., Taylor,A.F. and Smith,G.R. (2020) Chi hotspot control of RecBCD helicase-nuclease by long-range intramolecular signaling. *Sci. Rep.*, **10**, 19415.
44. Nyitrai,M. and Geeves,M.A. (2004) Adenosine diphosphate and strain sensitivity in myosin motors. *Philos. Trans. R. Soc. Lond. B Biol. Sci.*, **359**, 1867–1877.
45. Hannemann,D.E., Cao,W., Olivares,A.O., Robblee,J.P. and De La Cruz,E.M. (2005) Magnesium, ADP, and actin binding linkage of myosin V: evidence for multiple myosin V–ADP and actomyosin V–ADP states. *Biochemistry*, **44**, 8826–8840.
46. Zananiri,R., Malik,O., Rudnizky,S., Gaydar,V., Kreiserman,R., Henn,A. and Kaplan,A. (2019) Synergy between RecBCD subunits is essential for efficient DNA unwinding. *eLife*, **8**, e40836.
47. Simon,M.J., Sokoloski,J.E., Hao,L., Weiland,E. and Lohman,T.M. (2016) Processive DNA unwinding by RecBCD helicase in the

absence of canonical motor translocation. *J. Mol. Biol.*, **428**, 2997–3012.
48. Wu,C.G., Xie,F. and Lohman,T.M. (2012) The primary and secondary translocase activities within E. coli RecBC helicase are tightly coupled to ATP hydrolysis by the RecB motor. *J. Mol. Biol.*, **423**, 303–314.
49. Velankar,S.S., Soultanas,P., Dillingham,M.S., Subramanya,H.S. and Wigley,D.B. (1999) Crystal structures of complexes of PcrA DNA helicase with a DNA substrate indicate an inchworm mechanism. *Cell*, **97**, 75–84.
50. Lee,J.Y. and Yang,W. (2006) UvrD helicase unwinds DNA one base pair at a time by a two-part power stroke. *Cell*, **127**, 1349–1360.
51. Cheng,K., Wilkinson,M., Chaban,Y. and Wigley,D.B. (2020) A conformational switch in response to Chi converts RecBCD from phage destruction to DNA repair. *Nat. Struct. Mol. Biol.*, **27**, 71–77.
52. Liu,B., Baskin,R.J. and Kowalczykowski,S.C. (2013) DNA unwinding heterogeneity by RecBCD results from static molecules able to equilibrate. *Nature*, **500**, 482–485.
53. Wigley,D.B. (2000) DNA helicases: one small step for PcrA, one giant leap for RecBC?. *Curr. Biol.*, **10**, R444–R446.
54. Niedziela-Majka,A., Chesnik,M.a., Tomko,E.J. and Lohman,T.M. (2007) Bacillus stearothermophilus PcrA monomer is a single-stranded DNA translocase but not a processive helicase in vitro. *J. Biol. Chem.*, **282**, 27076–27085.
55. Lee,K.S., Balci,H., Jia,H., Lohman,T.M. and Ha,T. (2013) Direct imaging of single UvrD helicase dynamics on long single-stranded DNA. *Nat. Commun.*, **4**, 1878.
56. Ali,J.A., Maluf,N.K. and Lohman,T.M. (1999) An oligomeric form of *E. coli* UvrD is required for optimal helicase activity. *J. Mol. Biol.*, **293**, 815–834.
57. Bianco,P.R., Kowalczykowski,S.C., Blanco,P.R., Kowalczykowski,S.C., Bianco,P.R. and Kowalczykowski,S.C. (2000) Translocation step size and mechanism of the RecBC DNA helicase. *Nature*, **405**, 368–372.
58. Pavankumar,T.L., Wong,C.J., Wong,Y.K., Spies,M. and Kowalczykowski,S.C. (2024) Trans-complementation by the RecB nuclease domain of RecBCD enzyme reveals new insight into RecA loading upon χ recognition. *Nucleic Acids Res.*, https://doi.org/10.1093/nar/gkae007.
59. Fazio,N.T., Mersch,K.N., Hao,L. and Lohman,T.M. (2024) *E. coli* RecB nuclease domain regulates RecBCD helicase activity but not single-stranded DNA translocase activity. *J. Mol. Biol.*, **436**, 168381.

Received: May 22, 2023. **Revised:** January 30, 2024. **Editorial Decision:** January 31, 2024. **Accepted:** February 5, 2024